JOURNAL OF SPACECRAFT AND ROCKETS
Vol. 45, No. 5, September–October 2008

Solar Array Plasma Interaction: Influence of Interconnect Shape on Primary Arc Parameters

Justin J. Likar* and Alexander Bogorad†
Lockheed Martin Commercial Space Systems, Newtown, Pennsylvania 18940

DOI: 10.2514/1.35524

When immersed in a low Earth orbit-like plasma environment, including that generated by electric propulsion thrusters such as arcjets, Hall current thrusters, or ion thrusters, negatively biased solar cells are susceptible to arcing, typically initiated at triple point locations. The physical mechanisms for, and modeling of, primary (trigger) arc generation have been studied previously in detail by numerous authors and institutions. However, the particular influence of solar cell interconnector shape remains to be explored in a high level of quantitative detail at bias voltages achievable by typical Earth-orbiting spacecraft. The present study focuses on the specific influence of the strain-relief and *Z*-bend interconnector shapes on commonly characterized solar array arcing parameters of onset voltage and arc rate at representative bias voltages within realistic plasma environments. Results yielded quantitatively significant findings, indicating that specific designs are susceptible to arc inception at bias voltages readily achievable at near Earth orbits.

Nomenclature

A	=	area of coverglass edge under electron bombardment
d	=	height of solar cell coverglass
d_{CL}	=	child Langmuir distance
E_n	=	electric field normal to coverglass edge surface
$E_{n'}$	=	enhanced electric field normal to coverglass edge surface
E_t	=	electric field tangential to coverglass edge surface
e	=	electron charge
l_c	=	length of coverglass
l_i	=	distance between coverglasses
m_e	=	electron mass
m_n	=	neutral mass
N_t	=	emission/reabsorption multiplication factor
n_e	=	electron number density
n_n	=	neutral number density
T_e	=	electron temperature
T_s	=	surface temperature of coverglass
U_{pl}	=	plasma potential
V_t	=	arc threshold voltage
v_n	=	neutral gas velocity
γ	=	ratio of neutral gas specific heats
ε_0	=	permittivity of free space
λ_D	=	Debye length
λ_{mfp}	=	electron mean free path
ξ_0	=	mean energy of secondary electron emitted from coverglass
$\xi_{1,2}$	=	energies at which secondary electron yield equals exactly unity
σ_{ion}	=	ionization cross section
Γ	=	desorption efficiency

Received 6 November 2007; revision received 2 April 2008; accepted for publication 3 April 2008.

*Senior Design Engineer, Lockheed Martin Space Systems Advanced Technical Leadership Development Program. Member AIAA.
†Senior Staff Engineer.

Introduction

PHOTOVOLTAICS are used in a wide variety of spacecraft applications and orbits/trajectories. Solar arrays are included in designs of Earth-orbiting spacecraft at low Earth orbits (LEO), geosynchronous Earth orbits (GEO), middle Earth orbits (MEO), and Molniya orbits, as well as on deep space/planetary exploration missions, at a wide range of operating voltages. Consequently, solar array designs, which include many common elements, must be designed for operation in a variety of natural and thruster-generated plasma environments.

A spacecraft behaves like an isolated electrical probe when immersed in the space plasma environment. An electrical probe in a plasma the vehicle will collect charge and acquire an electrostatic potential as determined by Maxwell's equations. The spacecraft floating potential will reach an equilibrium value determined by the current balance to its exterior surfaces. The ultimate value and the time it takes the spacecraft to reach the equilibrium potential is influenced by several factors, including surface area size, photoemissive properties, secondary electron emission properties, and surface resistivity of exterior materials. Spacecraft operating in geostationary orbit are routinely charged negatively by the ambient plasma environment, with potentials of several hundred to several thousand volts readily achievable. If, during the time period when the spacecraft is charged negatively, electric propulsion attitude control thrusters are used, there may be an increased propensity for arcing on the spacecraft solar arrays due to the enhanced plasma environment created by the thruster plumes. The operating thrusters create an environment more closely resembling the higher density conditions at LEO than the cold, tenuous, ambient GEO environment.

The response of a negatively biased solar array in natural and electric propulsion (EP) generated plasma environments has been well characterized previously by the authors and others [1–3]. When immersed in a low Earth orbit-like plasma environment, including that generated by EP thrusters such as arcjets, Hall current thrusters (HCT), or ion thrusters, negatively biased solar cells are susceptible to arcing. As described in detail by [4–7], authored by Hastings et al., Cho and Hastings, and Vayner et al., arcs are typically initiated at triple point or exposed metal/semiconductor locations. The triple point is defined as a point at which plasma, a high-voltage conductor, and an insulator come together; at such a point, the electric field is often at a maximum [8]. This low-energy arcing can, if conditions are appropriate, initiate damaging extended or secondary arcs, as well as potentially catastrophic sustained arcs that burn until the current source is removed. Such phenomena have been the theorized cause

for numerous solar array or power system anomalies on board geosynchronous Earth-orbiting spacecraft [9–11] and, hence, are a topic of great interest to spacecraft designers, operators, and insurers. The physical mechanisms for, and modeling of, primary (trigger) arc generation have been studied previously in detail [4–7]; however, the particular influence of solar cell interconnector shapes (strain relief and *Z*-bend) remains to be explored in a high level of quantitative detail at bias voltages achievable by typical GEO spacecraft.

The importance of understanding the causes of, and characterizing the effects of, low power primary arcs is often underestimated when compared with the effects of high current and higher power secondary and sustained arcs, which can result from primary arcs in some cases. To optimize solar array designs for near Earth and deep space missions, it is necessary to achieve a thorough understanding of the potential effects of possibly thousands of low power arcs [12]. Detailed effects are not discussed further herein but may include cumulative damage to solar cells, decreased power output, contamination, and more.

Vayner and Ferguson [6,7] have noted the importance of the metallic interconnector in their description of the triple point arc inception mechanism. As noted in [3], solar array designs, which included strain-relief or looped interconnectors, were observed during ground testing to experience lower primary arc threshold voltages than designs that included in-plane interconnectors; however, only limited results for bias voltages less than −100 V were published previously. Furthermore, Likar et al. [3] did not present detailed analytical and/or theoretical models that describe the observed influence on arc inception level due to interconnector shape. Such models are introduced herein, along with new ground test data that characterize, in detail, interconnector shape-induced effects on arc inception voltage and arc rate at low bias voltages (−10 to −200 V) in plasma environments that represent conditions of LEO and arcjet engine plumes. Several factors influence the selected shapes of interconnectors. However, that which most often results in the selection of strain-relief or looped interconnectors is tolerance for thermal and mechanical stress; refer to Chap. 6 of Rauschenbach [13] for a detailed discussion of interconnector design considerations.

Experimental Setup

All testing was performed in a simulated LEO-like plasma environment in multiple vacuum chambers with similar vacuum, plasma generation, and plasma diagnostics capabilities. Because data presented herein were obtained in the process of a solar array plasma interaction study of larger scope, testing was performed in multiple phases using laboratories that included the NASA Glenn Research Center Plasma Interaction Facility (GRC PIF) in Cleveland, Ohio, and the Lockheed Martin Commercial Space Systems Plasma Interaction Facility (LM PIF) in Newtown, Pennsylvania. Both facilities included vacuum equipment capable of generating background vacuum pressures of less than 1 μtorr. A single hollow cathode, or Kaufmann ion source (depending on test facility) was used to generate a xenon plasma of electron density $n_e = 0.1\text{–}10 \times 10^5$ cm^{-3} and temperature $T_e = 1.0\text{–}1.5$ eV, whereas the measured xenon neutral gas pressure of $5\text{–}7 \times 10^{-5}$ torr was steady throughout testing. Plasma diagnostics were similar at both test facilities and included the use of at least one Langmuir probe (LP) and retarding potential analyzer (RPA) for the purposes of empirical determination of plasma parameters. Typical test conditions in the GRC PIF vacuum vessel resulted in a Debye length (λ_D) found to be ∼1.5 cm with an estimated plasma sheath size of $d_{\mathrm{CL}} \approx 125$ cm at −600 V. Similarly, a typical Debye length, as found for the LM PIF vacuum vessel, was found to be ∼1.0 cm with an estimated plasma sheath size of $d_{\mathrm{CL}} \approx 100$ cm at −600 V. As both chambers are more than 1 m in diameter, wall effects are minimized for potentials of −300 V and greater.

Coupons 1, 2, 4, and 5 were tested in the NASA GRC PIF vacuum chamber, whereas coupons 3 and 6 were tested in the LM PIF vacuum chamber. Sample(s) under test were mounted vertically in the middle of the vacuum chamber, as shown in Fig. 1, and were biased via a high-voltage power supply through the test circuit shown in Fig. 2. Electronic diagnostics included two current probes of varied bandwidths to measure and record primary discharge current, and a single voltage probe was used to measure and record the voltage pulse during the discharge. Although not a primary focus of the present study, arc sites were determined via the use of one or more vacuum-compatible video cameras and a digital recording system. All testing was performed at room temperature with samples held under high vacuum conditions for at least 24 hr before testing to minimize the effects of outgassed materials. A common test procedure was used for all samples:

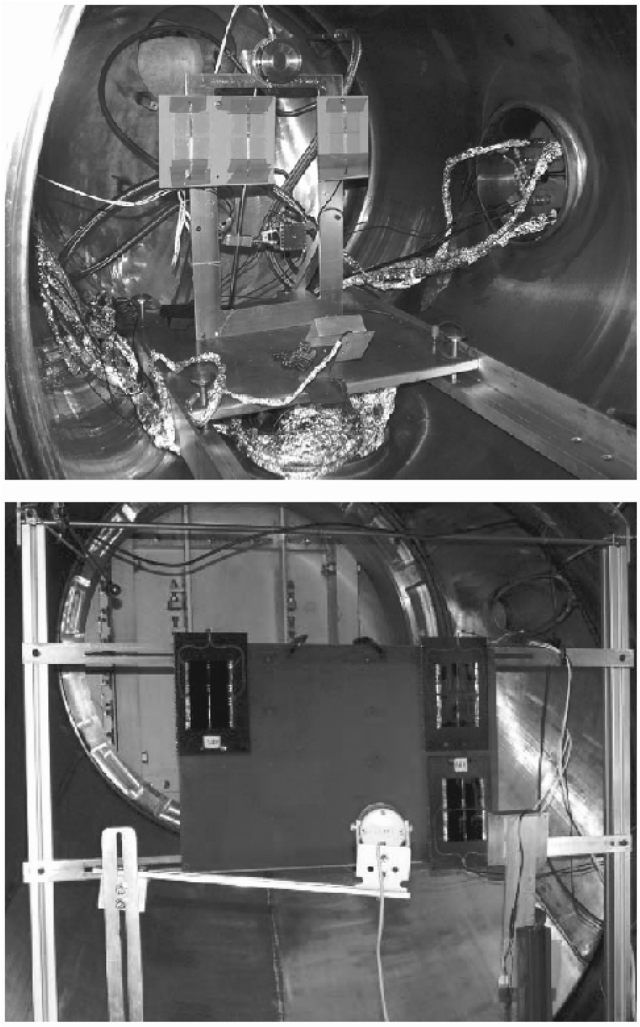

Fig. 1 Photographs of coupons as installed in vacuum chambers. Coupons as mounted in LM PIF vacuum chamber (top) and GRC PIF vacuum chamber (bottom). Photograph at bottom contains additional samples with test results not discussed herein. The LM PIF vacuum chamber includes a hollow cathode plasma source (not shown), whereas the GRC PIF includes a Kauffman plasma source (also not shown).

1) The string under test is biased negatively, relative to the plasma, to a voltage presumed to be well below the arc inception threshold.

2) A 15–30 min dwell time interval is allowed to collect arcs should they occur.

a) Primary arc time and oscilloscope current/voltage traces are recorded.

b) Primary arc location is recorded via video monitoring system.

3) The bias magnitude is increased by 10–20 V.

Table 1 provides a summary of the two simulated solar cell coupons and four engineering coupons used during ground testing. The simulated solar cell coupons were created without metallic turnarounds to ensure that all arcing occurred at the interconnector location. Engineering test coupons were selected to emphasize the effects of interconnector shape on primary arcing parameters.

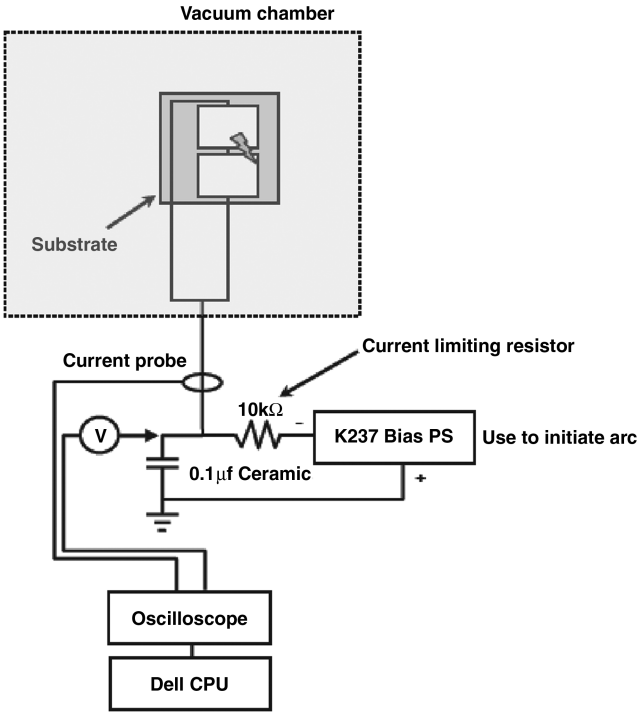

Fig. 2 Diagram of test setup. A negative bias is applied to the string under test through an RC circuit (0.1 μF ceramic capacitor and 10 kΩ resistor).

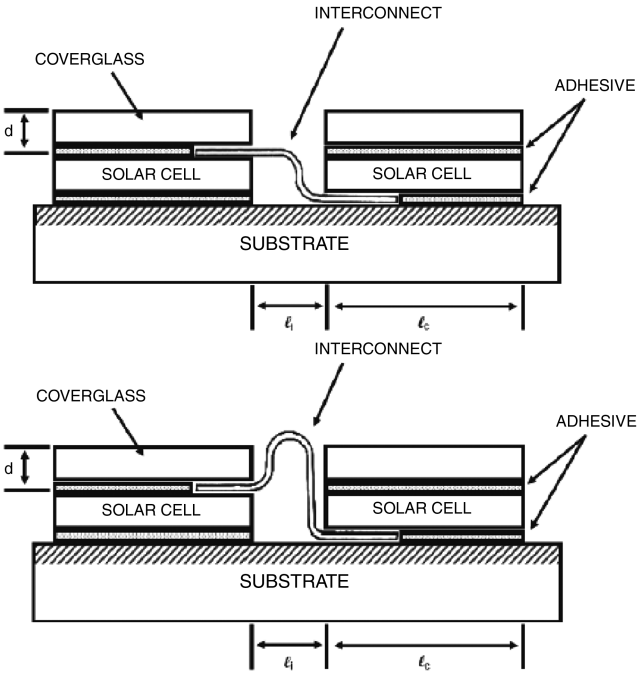

Fig. 3 Identification of key solar cell dimensions and characteristics. Geometric structure of cell/interconnect/coverglass/substrate/plasma interface; *Z*-bend interconnect is shown at top and strain-relief interconnect is shown at bottom.

Diagrams highlighting key elements and dimensions of the solar array coupon designs are shown Fig. 3, whereas detailed digital photographs of the interconnect shapes are shown in Figs. 4 and 5. Photographs shown in Fig. 4 represent a simulated solar cell/coverglass stack up, which excludes the actual solar cell but includes spaceflight quality adhesives and coverglasses; alternatively, Fig. 5 shows engineering test coupons, which include all space flight quality components.

Laboratory coupons (coupons 3 and 6), shown in Fig. 4, were constructed using simulated 4 × 6 cm solar cells. To eliminate any noninterconnector metal from the test coupon, cells were simulated with G10 glass epoxy fabric of thickness 0.127 mm (5 mil), whereas solar cell interconnectors were simulated using 99.95% purity silver of thickness 0.127 mm (5 mil) and width ∼3 mm (0.125 in.). The dimensions of the simulated interconnectors were engineered to accurately simulate those found on the engineering test coupons, and consequently on flight solar array designs. Uncoated borosilicate solar cell coverglasses were used in cell/interconnect/coverglass (CIC) construction with thickness of 0.15 mm (6 mil), whereas ∼0.0254 mm (1 mil) thick silicone adhesives were used to bond all layers.

All four engineering test coupons included a total of four solar cells electrically connected to form two independently powered strings. The engineering test coupons do not represent ideal or laboratory samples but rather typical construction for common space applications. As shown in Table 1, multijunction GaAs or single-junction silicon solar cells were used in coupon construction with typical cell thicknesses of 0.127 mm (5 mil). Coupons 1 and 2 included 4 × 6 cm rectangular standard single-junction silicon cells, whereas coupons 4 and 5 included nonrectangular or amorphous cells described in more detail in [3]. All interconnects on the engineering test coupons were silver coated with a substrate of another (known but variable) metal, whereas coverglasses were also uncoated borosilicate glass of 0.15 mm (6 mil) thickness. Interconnect thickness is identical to those on laboratory coupons with widths of each toe smaller at ∼1.5 mm (0.062 in). Nominal coverglass overhangs of 0.076 mm (3 mil) to 0.178 mm (7 mil) were present on all test coupons. Adhesive bond thicknesses were nearly identical to those described previously for the laboratory samples. Spacing between solar cells was nominally 0.127 mm (5 mil) to 0.508 mm (20 mil) and quite representative of typical space applications.

Experimental Results

All coupons were observed to arc readily in the simulated plasma environment, with measurably lower arc inception voltages observed on those coupons that included looped or strain-relief interconnectors. All arcs which occurred on coupons 3 and 6 were verified both visually and via coupon design to have occurred at the interconnector location. Visual observations and review of the digital video test recordings were used to verify that all, or very nearly all, arcs observed during the testing of coupons 1, 2, 4, and 5 occurred at the interconnector triple point sites. As summarized in Figs. 6 and 7, primary arcs were observed at negative bias voltages less than 100 V; specifically, multiple arcing events were observed at bias voltages of

Table 1 Summary of coupon descriptions

Coupon	Cell type	Interconnector type	Manufactured/fabricated	Number of cells
1	Standard si 4 × 6 cm	*Z*-bend	Stock	4
2	Standard si 4 × 6 cm	*Z*-bend	Stock	4
3	Simulated 4 × 6 cm	*Z*-bend	Laboratory	2
4	GaAs amorphous[a]	Loop	Stock	4
5	GaAs amorphous[a]	Loop	Stock	4
6	Simulated 4 × 6 cm	Loop	Laboratory	2

[a]Amorphous shaped cells described in detail by [3].

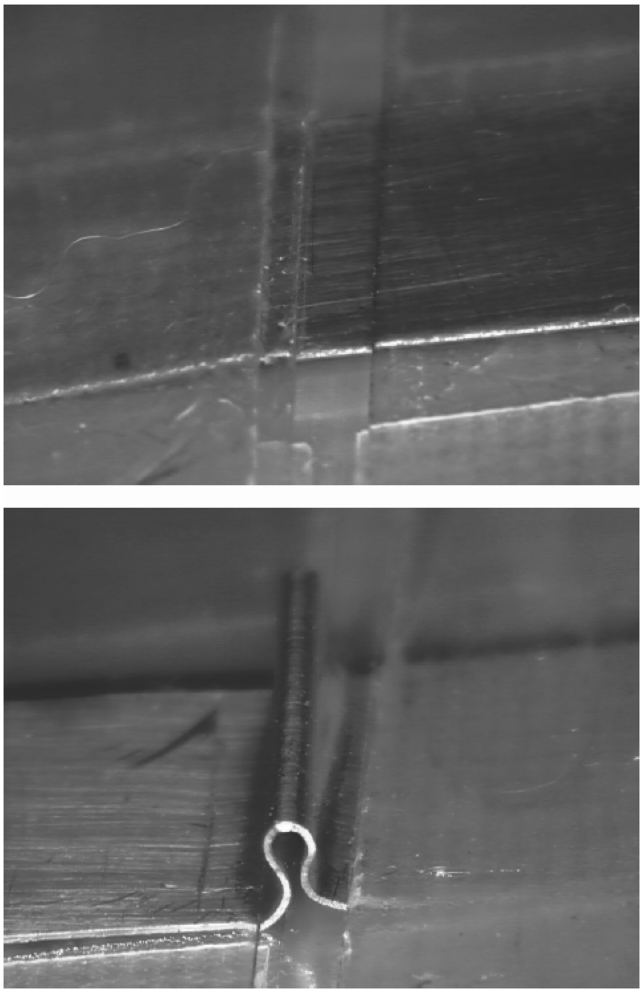

Fig. 4 Interconnector types. Digital photographs of (simulated) cell/interconnect/coverglass (CIC)/substrate/plasma interface; *Z*-bend interconnect is shown at top and strain-relief interconnect is shown at bottom.

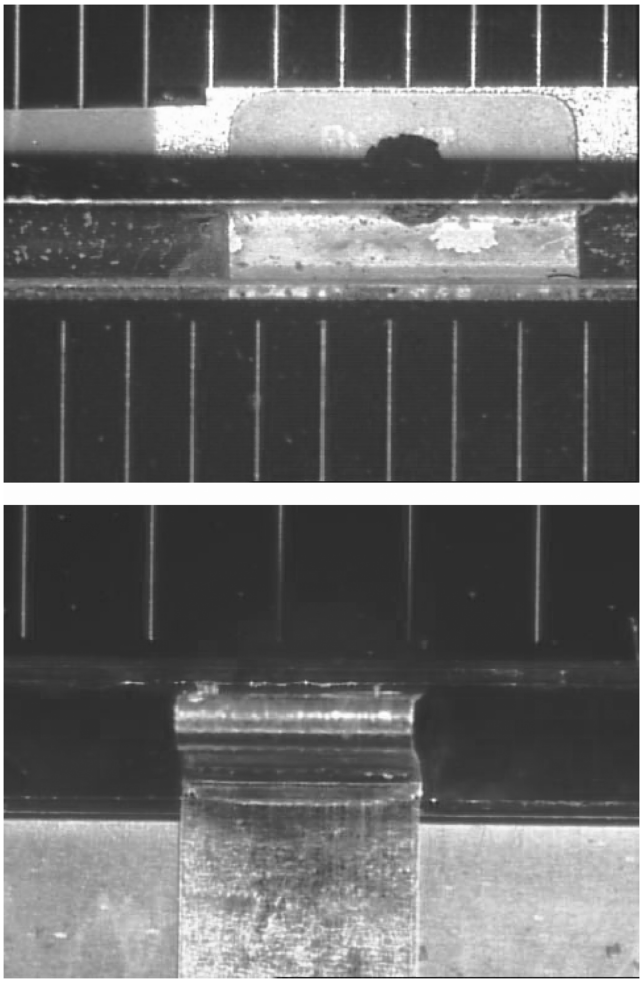

Fig. 5 Interconnector types. Digital photographs of cell/interconnect/coverglass (CIC)/substrate/plasma interface; *Z*-bend interconnect is shown at top and strain-relief interconnect is shown at bottom.

−70 V. Such results are quantitatively significant, as negative bias voltages of several hundred volts are typical for geostationary orbiting spacecraft [3] although precise bias voltages for a particular system will be dependent on various spacecraft, surface, and grounding properties. Arcing observed at negative bias voltages less than 100 V would be indicative of a design that is quite susceptible to arcing.

The lowest arc inception voltage observed on the nonlaboratory coupons, which include the *Z*-bend interconnect shape, was approximately −250 V, or 3–4 times the arc inception voltage of the nonlaboratory coupons, which included the looped interconnector design. A similar, but lesser, quantitative ratio (∼2 times) is recognizable for the primary arc threshold voltage for the laboratory coupons (nos. 3 and 6), although the actual values are measurably higher. The observed arc rates of 10^{-3} to 10^{-1} s^{-1} are in line with those published by Ferguson in [14].

As noted in the previous paragraph, noticeably higher negative bias voltages were required to generate primary arcs on the laboratory coupons that excluded the presence of solar cells and also limited the total number of triple point sites to one per coupon. It is proposed by the author that the resulting 4 to 12 times reduction in triple point sites (arc sites) was the determining factor in the observed increase in primary arc threshold voltage. A second, notable factor that may also have contributed to this observation includes manufacturability influences whereby laboratory-fabricated coupons may have resulted in less manufacturing-generated defects, primarily being surface roughness (such as burrs, scratches, and pitting) in metallic interconnectors, which are known arc sites. Such

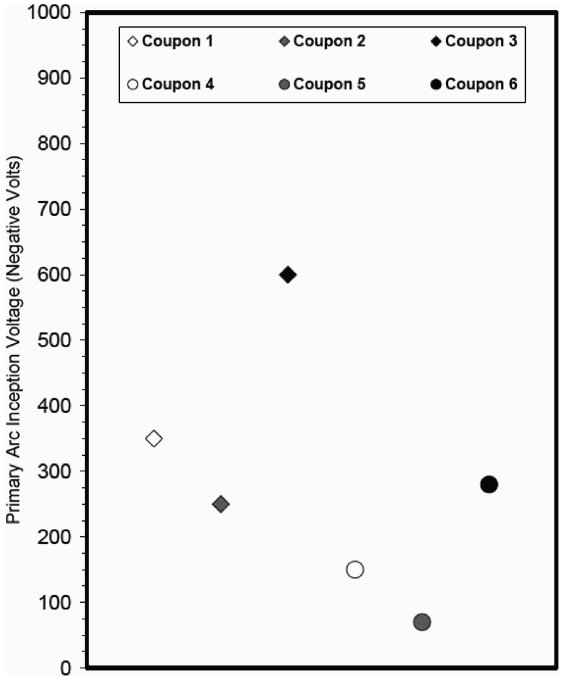

Fig. 6 Measured arc inception voltage. Coupons 1–3 include the *Z*-bend interconnector shape whereas coupons 4–6 include the strain-relief interconnector shape.

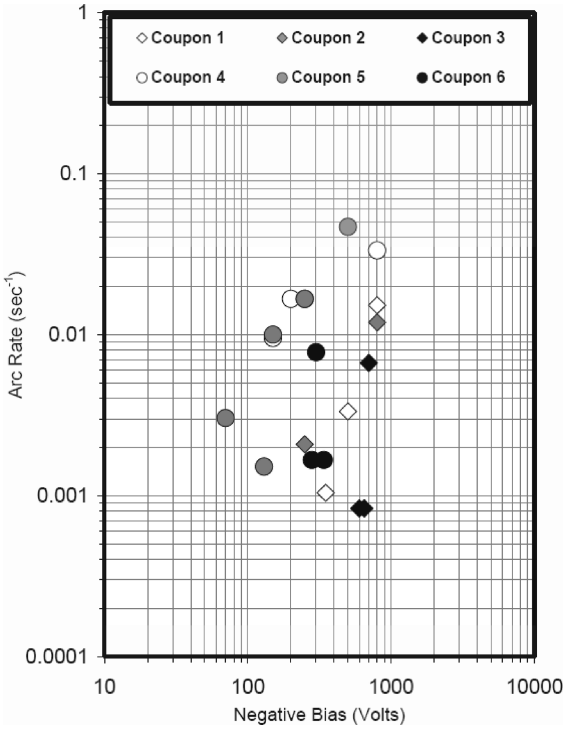

Fig. 7 Measured arc rate for all coupons. Coupons 1–3 include the Z-bend interconnector shape whereas coupons 4–6 include the strain-relief interconnector shape.

manufacturability defects, however, should not be discounted, as they should be expected when considering practical spacecraft manufacturing, assembly and test applications because they would be realistically expected on all manufactured solar arrays and spacecraft and, therefore, present on orbit; the impacts of such defects should be included in all ground testing such as that summarized herein.

Theoretical Analysis

The following discussion of primary arc inception is based on the well-developed model by Hastings et al. [4], Cho and Hastings [5], and Vayner et al. [6,7]. Only the derivation highlights of the equation describing the minimum breakdown voltage [4] are summarized here. Only portions of the derivation necessary to introduce features, processes, and details sufficient to describe the effects of the looped interconnect on the breakdown voltage are identified.

As always, precursors to breakdown include the presence of a negatively biased conductor (the interconnect or solar cell edge) in the presence of a plasma and, based on prior experimental results, electron current flow from the conductor to the coverglass. The basic model is that neutral gas is desorbed, via electron-stimulated desorption, from the coverglass because of bombardment from electrons and ions. Electrons that impact the coverglass sides originate both from the current flow from the interconnect as well as from secondary electrons, which are emitted from the coverglass under bombardment from the primary electrons and return to strike the glass surface. The phenomena of electron bombardment is sufficient to cause desorption of neutral gas molecules via electron-stimulated desorption [4,6,7]. A portion of the desorbed gas accumulates in the gap between coverglasses, where it forms a higher pressure region that can break down in the presence of the continuing electron current from the conductor.

The lower bound on the primary arc threshold voltage is given by

$$V_t = \left[0.60\frac{e}{\varepsilon_0}\left(\frac{d}{\ell_i}\right)\left(\frac{\gamma T_s/e}{2m_n/m_e}\right)^{1/2}\frac{(\xi_1-\xi_0)d}{\Gamma\sigma_{\text{ion}}e}\right]^{2/5} \qquad (1)$$

in the space charge limit for current, which can be pulled from the metallic interconnect. The relationship in Eq. (1) is recognized as

Table 2 Parameter values used in calculation of primary arcing onset voltage per Eq. (1)

Parameter	Value	Units
T_s	300	K
	0.0258	eV
m_n	44	amu
	7.3×10^{-26}	kg
m_e	5.5×10^{-4}	amu
	9.11×10^{-31}	kg
ξ_1	40	eV
ξ_0	2	eV
d	0.15	mm
l_i	1.5	mm
Γ	0.03	——
	0.003	——
σ_{ion}	1×10^{-20}	m^2
	1×10^{-16}	cm^2
γ	1.2	——
e	1	eV
	1.6×10^{-19}	C

Eq. (11) of [4], in which it is assumed that the gas flow out of the interconnect-coverglass region is choked [4]. Typical values of some variables in Eq. (1) are shown in Table 2; values for some parameters are selected from [4,5,15,16], whereas values for other parameters have been selected based on coupon characteristics used in studies reported herein. Using the variable values summarized in Table 2, some of which are order of magnitude estimates, one finds a threshold voltage of ~600 V negative for Γ of 0.03, a value that is not unreasonable when compared with recent empirical data.

Equation (1) and the physical method described herein offer quite good agreement to the empirical data for CIC configurations, which employ flat, or nearly flat, interconnects as shown in left-hand side of Figs. 3–5. A slight modification to the derivation and physical method is required to treat the case of the strain-relief interconnect shown in the right-hand side of Figs. 3–5. The presence of the strain-relief interconnector loop results in an enhancement of the electric field normal to the coverglass side surface as shown in Fig. 8. The resulting, enhanced normal electric field (E'_n) will be dependant on the geometry of the interconnector, which, due to normal manufacturing uncertainties, will vary somewhat in height and angle relative to the coverglass side surface. Nonetheless, the enhanced normal electric field can be expected to be approximated as

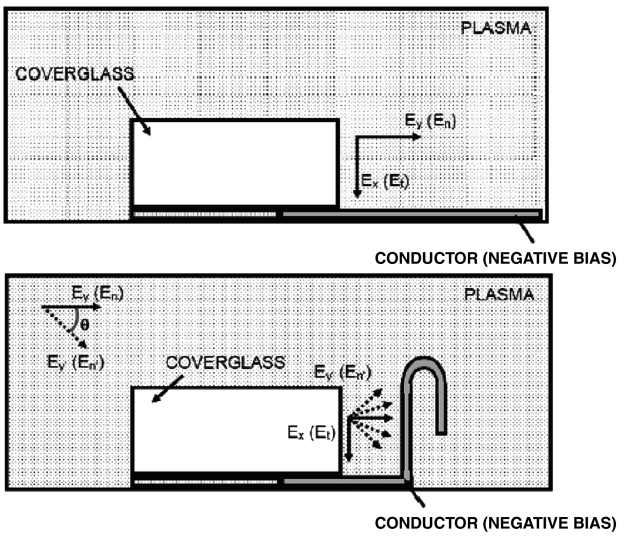

Fig. 8 Relevant electric fields in electron-simulated desorption and primary arc generation. Cartoon representation of electric fields present at cell/interconnect/coverglass (CIC)/substrate/plasma interface; Z-bend interconnect shown at top and strain-relief interconnect shown at bottom. Presence of strain-relief loop results in an enhancement of the electric field normal to the coverglass side surface.

$E_{n'} \approx E_n(1 + \varepsilon_{ne} \cos\theta)$, where the angle θ is defined as the angle between the resultant enhanced normal electric field and the normal electric field without the presence of the looped interconnector, and the enhancement factor ε_{ne} can be estimated as described by the following method. Clearly, this relationship behaves as necessary at the limiting values of θ, in approaching the "nonenhanced" value of E_n at $\theta = 90$ deg and approaching $1 + \varepsilon_{ne}$ for $\theta \to 90$ deg.

The effect of the strain-relief interconnector and the enhanced electric field at the interconnector/substrate/plasma triple point interface can be effectively illustrated via the use of the NASA Charging Analyzer Program (NASCAP-2k) software [17]. NASCAP-2k,, developed by Science Applications International Corporation (SAIC) as part of a program sponsored jointly by the Air Force Research Laboratory (AFRL) and NASA's Space Environments and Effects (SEE) Program, includes capabilities for studying various spacecraft plasma interactions in both tenuous (GEO/interplanetary) and dense plasma (LEO) environments. Potentials-in-space calculations were performed to model the resulting equipotential contours surrounding three dimensional models of biased CICs in GEO plasma conditions using both *Z*-bend and strain-relief looped interconnectors. Figures 9 and 10 include the results of simulations in which the interconnector was biased to a typical bus operating voltage (+75 V) and placed in a worst-case GEO plasma environment [18]. Simulations shown in Figs. 9 and 10 are representative of the electric fields present for several seconds at the start of thruster operation when a spacecraft is charged negatively due to the natural GEO environment; such a condition is described by Likar et al. [3]. Cutplanes at the interconnector reveal that, as expected, a strong potential gradient is formed in the dense region between the coverglasses when the looped interconnector is used. The electric field enhancement normal to the coverglass side surface can be estimated in one dimension via

$$\varepsilon_{ne} = -\nabla V = -\frac{dV}{ds} \tag{2}$$

where, from Fig. 10 dV is estimated as 55 V and ds is estimated as the distance between the interconnector surface and the coverglass side surface or approximately 0.05 m. The resulting estimation for electric field enhancement is found to be $\sim$1000 V/m.

Including such an enhancement factor as part of the physical mechanism for primary arc breakdown results in a modification to the relationship which describes the ratio of tangential and normal electric fields in which the assumption is maintained that the ratio of tangential and normal electric fields, now with the enhanced normal electric field, produces an impact energy resulting in a secondary electron yield of one. For the strain-relief interconnector, however, the normal electric field is given by $E_{n'} \propto 1 + \varepsilon_{ne} \cos\theta$, where the value of ε_{ne} is approximately 1000 as approximated previously. Following through the derivation summarized here and by [4], one can arrive at a slightly modified equation for the minimum breakdown threshold:

$$V_t = \left[0.60 \frac{e}{\varepsilon_0}\left(\frac{d}{\ell_i}\right)\left(\frac{\gamma T_s/e}{2m_n/m_e}\right)^{1/2} \frac{(\xi_1 - \xi_0)d}{(1 + \varepsilon_{ne}\cos\theta)^2 \Gamma \sigma_{ion} e}\right]^{2/5} \tag{3}$$

It is clear that the electric field enhancement resulting from the presence of the strain-relief interconnector will act to reduce the minimum breakdown voltage and that the magnitude of the enhancement will be maximized when the interconnector geometry results in an enhanced electric field parallel with E_n. The resulting form of Eq. (3) behaves as desired when considering the limits of θ; as $\theta \to 90$ deg, the enhancement term $(1 + \varepsilon_{ne} \cos\theta)$ approaches 1 and V_t reduces to its original form of Eq. (1) for a flat interconnector. Conversely, when $\theta \to 0$ deg the enhancement term approaches $1 + \varepsilon_{ne}$, which is greater than 1, thereby forcing V_t to decrease to less negative bias values. Using the parameter values from Table 2 but including an enhancement factor of $\varepsilon_{ne} = 1000$, one finds that the breakdown voltage is reduced to under 10 V, or well over 100× less than the value calculated for the *Z*-bend interconnector. As an extension of the simplistic calculation described previously, Fig. 11 shows the behavior of Eq. (3) as a function of electric field enhancement factor and the angle between the resultant enhanced normal electric field and the normal electric field without the presence of the looped interconnector θ. It is recognized that only moderate enhancements in electric field of 5 times are necessary to result in a significant reduction in minimum arcing threshold voltage by a factor of 2 times. The limiting behavior of the relationship at

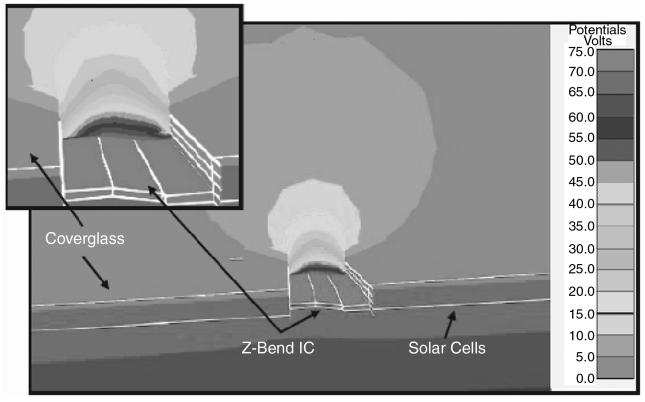

Fig. 9 Equipotential contours for in-plane interconnector. Equipotential contours resulting from +75 V bias on *Z*-bend interconnect in GEO plasma environment; cutplane through interconnector.

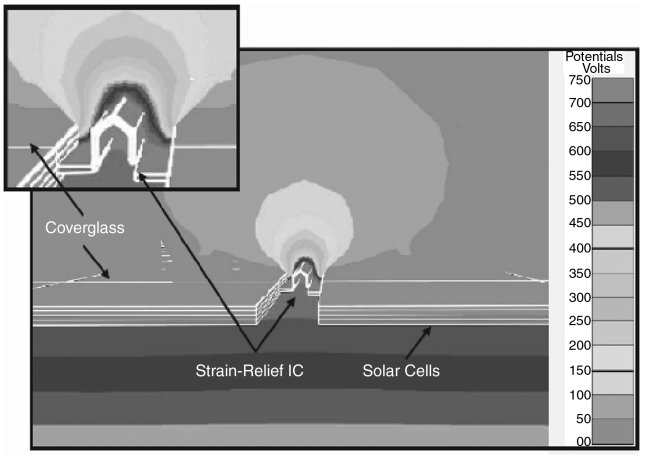

Fig. 10 Equipotential contours for strain-relief interconnector. Equipotential contours resulting from +75 V bias on strain-relief interconnect in GEO plasma environment; cutplane through interconnector.

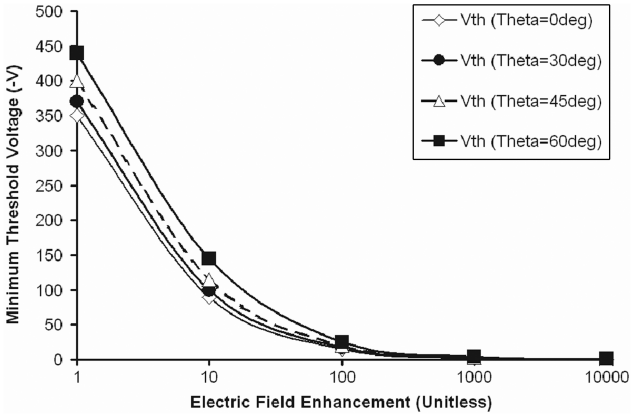

Fig. 11 Minimum arcing threshold voltage as calculated via Eq. (3) as a function of strain-relief interconnector electric field enhancement factor for various angles. The value reduces to the nonenhanced value of −600 V for zero enhancement factor and/or θ of 90 deg.

high enhancement factors is for trending purposes only; no higher order effects are included in this simple model to account for the limiting behavior as the arc inception voltage approaches zero. Arcing threshold values of less than 10 V negative are, in all likelihood, unrealistic; however, the theoretically determined relationship does serve to model the observed empirical data and establishes a first-order relationship between interconnector geometry and arcing threshold.

Conclusions

Results presented herein demonstrate the significant contributions to key solar array arcing parameters that result from variation in common, variable solar array design elements often overlooked during typical design activities. Empirical and theoretical results complimentarily indicate that the electric field enhancements introduced by strain-relief interconnector shapes are sufficient to reduce the primary arcing onset voltage significantly to values at or less than 100 V negative, depending on cell and coverglass properties; such negative biases are typical values encountered by most Earth-orbiting spacecraft.

It is pointed out, however, that the occurrence of primary (trigger) arcing alone is not a guaranteed precursor to degraded solar array performance and/or damaging high power secondary arcing, although the basic physical mechanisms for primary arc solar cell interactions are not fully understood, particularly in the instances of modern multiple junction solar cells. Nonetheless, results presented herein should assist solar array or space vehicle system designers seeking to create a system with optimized immunity to solar array plasma interactions wherefore the elimination or significant reduction of primary arcing offers a significant achievement in creating a robust solar array design. It is clear that, when not constrained by mechanical or thermal considerations, in-plane or near-in-plane interconnectors offer a quantitatively significant performance advantage over common looped interconnectors in terms of primary arcing susceptibility. Furthermore, results illustrate the interdependence of spacecraft design, solar array design, floating (chassis) potential, and arc inception voltage, and the beneficiary role that relevant plasma interaction analysis and ground testing plays when developing a robust solar array design for high reliability space power applications.

Acknowledgments

The author(s) are grateful to E. Choueiri and Y. Raitses of Princeton University for use of Princeton University Electric Propulsion and Plasma Dynamics (EPPDyL) and Princeton Plasma Physics Laboratory (PPPL) facilities during preliminary and intermediate testing. The author(s) would also like to thank M. Mandell and V. Davis of Science Applications International Corporation for consultations and discussions related to NASCAP-2k modeling.

References

[1] Stevens, J., "Review of Biased Solar Array: Plasma Interaction Studies," AIAA Paper 81-0738, 1981.

[2] Ferguson, D., "Solar Array Arcing in Plasmas," *NASA Conference Publication Third Annual Workshop on Space Operations Automation and Robotics*, NASA Office of Management and Technical Information Division, Washington, D.C., July 1989, pp. 509–513.

[3] Likar, J., Bogorad, A., Vayner, B., and Galofaro, J., "Influence of Solar Cell Shape, Interconnect Shape, and Coverglass Coatings on Solar Array Arcing Parameters," *Institute for Electrical and Electronics Engineers Nuclear and Space Radiation Effects Conference Data Workshop Record*, IEEE Publications, Piscataway, NJ, 2007, pp. 26–29. doi:10.1109/REDW.2007.4342535.

[4] Hastings, D., Weyl, G., and Kaufman, D., "Threshold Voltage for Arcing on Negatively Biased Solar Arrays," *Journal of Spacecraft and Rockets*, Vol. 27, No. 5, 1990, pp. 539–544.

[5] Cho, M., and Hastings, D., "Computer Particle Simulation of High-Voltage Solar Array Arcing Onset," *Journal of Spacecraft and Rockets*, Vol. 30, No. 2, 1993, pp. 189–201.

[6] Vayner, B., Galofaro, J., Ferguson, D., De Groot, W., and Vayner, L., "Arcing Onset on a Solar Array Immersed in a Low Density Plasma," AIAA Paper 01-0400, 2001.

[7] Vayner, B., Galofaro, J., and Ferguson, D., "Arc Inception Mechanism on a Solar Array Immersed in a Low Density Plasma," NASA TM-2001-211070, July 2001.

[8] "Low Earth Orbit Spacecraft Charging Design Standard," NASA STD-4005, June 2007.

[9] Katz, I., Snyder, D., and Robertson, E., "ESD Triggered Solar Array Failure Mechanism," Air Force Research Laboratory VS-TR-20001578, 2000, pp. 39–42.

[10] Ozkul, A., Cooper, D., and Dunnet, A., "In-Orbit Performance Characteristics of INTELSAT-V Solar Arrays," *Proceedings of the First World Conference of Photovoltaic Energy Conversion*, IEEE Publications, Piscataway, NJ, 1994, pp. 1994–1997. doi:10.1109/WCPEC.1994.520759.

[11] Toyoda, K., Matsumoto, T., Cho, M., Nozaki, Y., and Takahashi, M., "Power Reduction of Solar Arrays by Arcing Under Simulated Geosynchronous Orbit Environment," *Journal of Spacecraft and Rockets*, Vol. 41, No. 5, 2004, pp. 854–861. doi:10.2514/1.13103

[12] Cho, M., Kawakita, S., Nakamura, M., Takahashi, M., Sato, T., and Nozaki, Y., "Number of Arcs Estimated on Solar Array of a Geostationary Satellite," *Journal of Spacecraft and Rockets* Vol. 42, No. 4, 2005, pp. 740–748. doi:10.2514/1.6694

[13] Rauschenbach, H., "Electrical Elements," *Solar Cell Array Handbook*, Reinhold, New York, 1980, pp. 268–296.

[14] Ferguson, D., "Low Earth Orbit Spacecraft Charging Design Handbook," NASA HDBK-4006, June 2007.

[15] Anderson, R., and Brainard, J., "Mechanism of Pulsed Surface Flashover Involving Electron-Stimulated Desorption," *Journal of Applied Physics*, Vol. 51, No. 3, March 1980, pp. 1414–1421. doi:10.1063/1.327839

[16] Vayner, B., Galofaro, J., and Ferguson, D., "Interactions of High-Voltage Solar Arrays with Their Plasma Environment: Physical Processes," *Journal of Spacecraft and Rockets*, Vol. 41, No. 6, 2004, pp. 1031–1041. doi:10.2514/1.4271

[17] Mandell, M., Katz, I., Hilton, J., and Cooke, D., "NASCAP-2k: A Spacecraft Charging Analysis Code for the 21st Century," AIAA Paper 01-957,2001.

[18] Purvis, C., Garrett, H., Whittlesey, A., and Stevens, J., "Design Guidelines for Assessing and Controlling Spacecraft Charging Effects," NASA, TT 2361, 1984.

A. Ketsdever
Associate Editor